



Quantum Monte Carlo calculation of critical exponents of the Gross-Neveu-Yukawa on a two-dimensional fermion lattice model

Ting-Tung Wang and Zi Yang Meng ^{*}

*Department of Physics and HKU-UCAS Joint Institute of Theoretical and Computational Physics,
The University of Hong Kong, Hong Kong SAR, China*

 (Received 17 April 2023; revised 10 September 2023; accepted 11 September 2023; published 22 September 2023)

It is expected that the Gross-Neveu-Yukawa (GNY) chiral Ising transition of Dirac fermions coupled with a scalar field in $(2 + 1)$ dimensions will be the first fermionic quantum critical point that various methods, such as conformal bootstrap, perturbative renormalization group, and quantum Monte Carlo (QMC) simulations, would yield converged critical exponents—serving the same role as the Ising and $O(N)$ models in the textbooks of statistical and quantum physics. However, such an expectation has not been fully realized from the lattice QMC simulations due to the obstacles introduced by the UV finite-size effect. In this Letter, by means of the elective-momentum ultrasize (EMUS)-QMC method, we compute the critical exponents of the $O(N/2)^2 \times \mathbb{Z}_2$ GNY $N = 8$ chiral Ising transition on a two-dimensional π -flux fermion lattice model between Dirac semimetal and quantum spin Hall insulator phases. With the matching of fermionic and bosonic momentum transfer and collective update in momentum space, our QMC results provide fully consistent exponents with those obtained from the bootstrap and perturbative approaches. In this way, the EMUS now live happily on the $N = 8$ island and could explore the chiral Gross-Neveu-Yukawa archipelago with ease.

DOI: [10.1103/PhysRevB.108.L121112](https://doi.org/10.1103/PhysRevB.108.L121112)

Introduction. Just as the Ising and $O(N)$ models are the simplest $(2 + 1)$ -dimensional $[(2 + 1)\text{D}]$ universality classes that the perturbative renormalization group (RG) analysis (ϵ expansion) [1,2], the conformal bootstrap [3–6], and lattice model simulations [7] have provided highly consistent and well-converged results—serving as the textbook example for the development of many-body methodologies, the simplest $(2 + 1)\text{D}$ universality class involving fermions—the Gross-Neveu-Yukawa (GNY) model of Dirac fermions coupled with a scalar bosonic field is expected to provide a similar level of consistency and bring our understanding of the quantum phase transitions in interacting Dirac fermion systems onto more solid ground.

Such consistency not only has a theoretical impact towards quantum field theory and high-energy physics [8–11], but is also intimately related to the ongoing research in d -wave superconductors and nematic quantum criticality [12,13], graphene [11,14–17], twisted bilayer graphene [18,19], and other quantum moiré materials [20,21], as well as the kagome metallic systems [22,23], where the transition from Dirac and Weyl semimetals (with the fermion flavor tuned by the spin, valley, and layer degrees of freedom and the Coulomb interaction tuned by gating and twist angles) to various symmetry-breaking phases holds the key to understanding the intriguing phenomena therein. However, such consistency, especially in the form of critical exponents or the scaling dimensions of external operators in the conformal field

theory (CFT) data, has not been fully reached for the simplest one—the GNY chiral Ising transition with $O(N/2)^2 \times \mathbb{Z}_2$ global symmetry. The present ϵ -expansion [10,11,24], conformal bootstrap with $O(N)$ global symmetry [9,25], and lattice model quantum Monte Carlo (QMC) simulations [26–31] are giving rise to closer exponents over the years (see Table I), except for the remaining boson anomalous dimension exponent η_ϕ . The $\sim 20\%$ deviation from the latest QMC study [26,27] compared with that from ϵ expansion [11,24] and conformal bootstrap [9] comes from the fact that, although in the latest lattice model simulation [26] the critical bosonic and fermionic modes are designed with the same velocity at the bare level, the actual coupled system when driving to the quantum critical point still acquires different velocities of the critical modes at the finite size studied (see Fig. 1 in Ref. [26]), and it has been observed that such a difference at the UV is sufficient to cause significant drifts of the exponents in the finite-size analyses (see Figs. 2 and 3 in Ref. [26]) and renders the access of the thermodynamic limit difficult. From these experiences, one sees that better model design and algorithmic developments, *with less computation time and human time*, are critically needed to overcome the problem and bring consistent results with bootstrap and ϵ expansion for GNY chiral Ising universality classes.

In this Letter, we achieve this goal by means of the elective-momentum ultrasize (EMUS)-QMC method [28,32,33]: We compute the critical exponents of the $N = 8$ chiral Ising GNY transition on a 2D π -flux fermion lattice model between Dirac semimetal (DSM) and quantum spin Hall insulator (QSH) phases [26,29]. By designing the matching of fermionic and bosonic momentum transfer within the high-resolution patches in the Brillouin zone (BZ) and a collective update

^{*}zymeng@hku.hk

TABLE I. EMUS live on the chiral Gross-Neveu-Yukawa archipelago. This table summarizes the critical exponents of the $N = 8$ chiral Ising GNY transition. We compare the EMUS-QMC results with previous QMC results and those from the latest ϵ -expansion and bootstrap estimates. The bootstrap estimates are obtained for the three external operators $\Delta_\epsilon = 3 - \frac{1}{\nu}$, $\Delta_\sigma = \frac{1+\eta_\phi}{2}$, and $\Delta_\psi = \frac{1+\eta_\psi}{2}$ of the GNY island with $O(8)$ global symmetry [9]. The ϵ -expansion work [24] relies on the DREG3 prescription to analytically continue spinors away from $d = 4$.

	$1/\nu$	η_ϕ	η_ψ
This work	1.07(12)	0.72(6)	0.04(2)
Previous QMC [26]	1.0(1)	0.59(2)	0.05(2)
Previous QMC [27]	1.20(1)	0.62(1)	0.38(1)
ϵ expansion [24]	0.993(27)	0.704(15)	0.043(12)
Conformal bootstrap [9]	0.998(12)	0.7329(27)	0.04238(11)

completely in the momentum space, we have effectively accessed much larger system sizes and better data quality with reduced computational cost as well as human time. Our QMC results yield the crossing of the RG-invariant ratio with very small drifts and our stochastic finite-size analysis finds fully controlled exponents (see Table I), finally in agreement with those obtained from the bootstrap and ϵ expansion.

With our computation protocol, the EMUS now live happily on the $N = 8$ island of the chiral GNY archipelago [9], and they can readily jump to other islands with a simple change of the simulation code and further explore the exciting and vast ocean of CFTs. Relevance towards the

experiment on interacting Dirac fermion systems is also discussed.

The chiral GNY model. At the level of field theory, our chiral GNY model describes the situation of an $N/4$ four-component Dirac interacting with a bosonic scalar field ϕ . The coefficient m in the $m\phi^2$ term of the bosonic Lagrangian [see Eq. (1)] has a critical value m_c , below which the bosonic scalar field spontaneously acquires a finite expectation value, giving a mass to the fermions [the QSH phase in Fig. 1(b)]. Above m_c , the expectation value of ϕ vanishes, and the fermions go back to the massless form [the DSM phase in Fig. 1(b)]. At m_c , the system is expected to flow to the chiral GNY CFT. We note in the literature there are two different GNY models with the same number of fermions but different global symmetry groups. In addition to the chiral GNY model with $O(N/2)^2 \times \mathbb{Z}_2$ global symmetry in this work, there is also the GNY model with $O(N)$ global symmetry investigated in a recent bootstrap work [9]. However, since these models are nearly degenerate and are only distinguishable at high perturbative order, the differences between the scaling dimensions of the external operators $\{\Delta_\psi = \frac{1+\eta_\psi}{2}, \Delta_\sigma = \frac{1+\eta_\phi}{2}, \Delta_\epsilon = 3 - \frac{1}{\nu}\}$ are very small ($\sim 3 \times 10^{-6}$) for $N = 1, 2, 4, 8$ [9,11], hence we focus on the lattice realization of the $N = 8$ chiral Ising GNY with $O(N/2)^2 \times \mathbb{Z}_2$ global symmetry.

We adapt the lattice model shown in Fig. 1(a) with the Lagrangian [26]

$$\mathcal{L} = \mathcal{L}_{\text{fermion}} + \mathcal{L}_{\text{boson}} + \mathcal{L}_{\text{coupling}}, \quad (1)$$

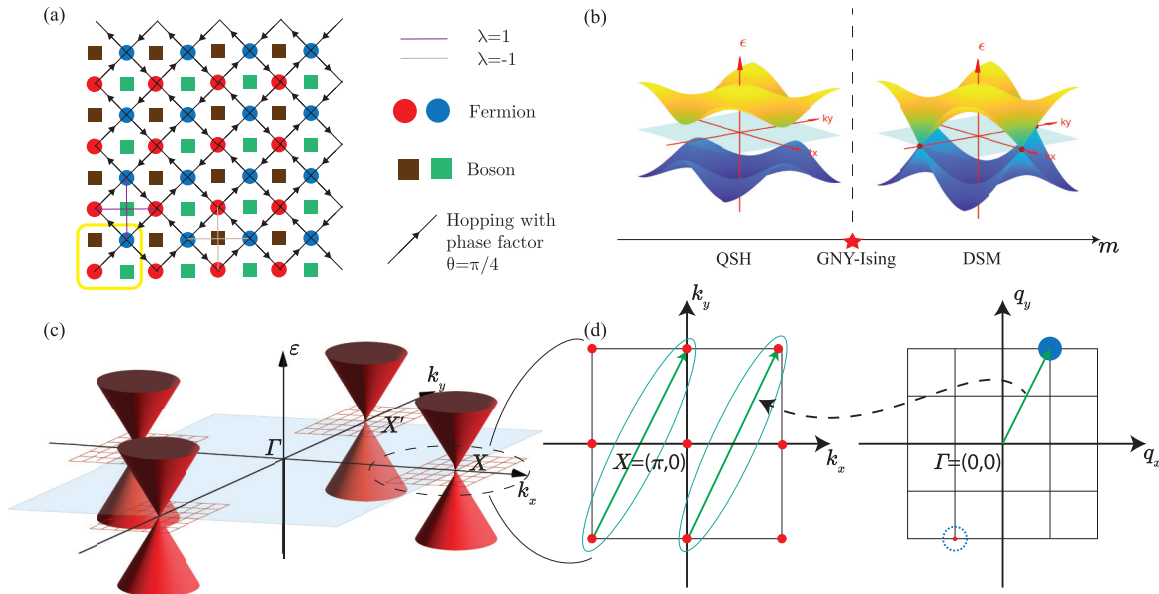


FIG. 1. Chiral-Ising GNY model and EMUS algorithm. (a) The lattice model of $N = 8$ chiral Ising GNY in real space. Each unit cell contains two boson and two fermion sites. Black arrows indicate fermionic hopping with phase factor $\theta = \frac{\pi}{4}$. Purple and beige lines indicate coupling terms with strength equal to the bosonic field multiplied with $\lambda = \pm 1$, depending on the boson sublattice. (b) Fermion dispersions. When m is small (large), bosonic fields are in ferromagnetic (paramagnetic) phases and the fermions are in the massive QSH (massless DSM) phases, separated by the GNY chiral Ising transition at m_c . (c) In momentum space, two patches near Dirac points are simulated in EMUS-QMC. (d) An example of the EMUS update scheme with patch size $L_f = 2$ (corresponds to $L = 12$ in the original model). The left panel is one of the patches in the fermion BZ. The right panel is the allowed momentum transfer for bosons.

where

$$\begin{aligned}\mathcal{L}_{\text{fermion}} &= \sum_{(i,j)\sigma} \psi_{i,\sigma}^\dagger [(i\partial_\tau - \mu)\delta_{ij} - t e^{i\sigma\theta_{ij}}] \psi_{j,\sigma} + \text{H.c.}, \\ \mathcal{L}_{\text{boson}} &= \sum_i \left[\frac{1}{4} \left(\frac{\partial\phi_i}{\partial\tau} \right)^2 + m\phi_i^2 + \phi_i^4 \right] + \sum_{(i,j)} J_{ij} (\phi_i - \phi_j)^2, \\ \mathcal{L}_{\text{coupling}} &= \sum_{\langle\langle i,j \rangle\rangle, \sigma} \lambda_{ij} \phi_p \psi_{i,\sigma}^\dagger \psi_{j,\sigma} + \text{H.c.},\end{aligned}$$

and $\psi_{i,\sigma}$ is the fermionic operator on each site i with spin $\sigma = \uparrow, \downarrow$. $\mathcal{L}_{\text{fermion}}$ describes fermions with nearest-neighbor hopping $t = 1$ and a phase factor $\theta = \pi/4$ for each bond, which introduces a π flux in each plaquette and leads to two Dirac cones at $X = (0, \pi)$ and $(\pi, 0)$ in the BZ. We set $\mu = 0$ to ensure the half filling of fermions.

In $\mathcal{L}_{\text{boson}}$, ϕ_i is the scalar bosonic field, and m is the mass term to tune the boson across the chiral GNY Ising transition. The imaginary time derivative term provides the quantum fluctuations. J_{ij} are interaction terms up to fourth-nearest neighbor, and their magnitudes are set to $J_1 = 4t^2/5$, $J_2 = -J_1/8$, $J_3 = J_1/63$, and $J_4 = -J_1/896$. This combination ensures the largest linear region in bosonic dispersion, and the bosonic velocity v_b is equal to that of the bare fermion $v_f = v_b = \sqrt{2}t$ [26].

$\mathcal{L}_{\text{coupling}}$ is a next-nearest-neighbor hopping for the fermion, whose strength is determined by the boson ϕ_p sitting on the bond and the difference of two boson sublattices $\lambda_{ij} = \pm 1$. In the symmetry-breaking phase of the bosonic field, this will open a gap at the Dirac points in fermion dispersion and transform the DSM to a QSH insulator [29].

We note that each of the two Dirac cones accounting for four fermion components (two spins and two sublattices), combining with the chiral symmetry consisting of the inversion of bosonic fields and swapping of the two sublattices, leads to a $O(4)^2 \rtimes \mathbb{Z}_2$ global symmetry.

EMUS-QMC method. As shown in Fig. 1(b), the linear dispersion of Dirac cones only occupies a small part of the BZ and simulating the region out of linear dispersion will not contribute much to the critical behavior. In previous studies, different methods have been introduced to bypass this issue. One can write the model with a single Dirac cone (the SLAC fermion) covering most of the BZ [30,34]. Although the SLAC fermion avoids the Nielsen-Ninomiya theorem [35,36], one has to pay the price of long-range hoppings and the violation of locality has been shown to fundamentally change the associated universality class [37–39]. One can also enlarge the linear dispersion region without violation of the locality, by adding longer neighbor hoppings with appropriate strength [26]. However, as discussed in the Introduction, one still experiences a strong finite-size effect when tuning the system to the interacting fixed point, and a drift in the crossings of RG-invariant ratios, and gives rise to the $\sim 20\%$ deviation of the bosonic anomalous dimension η_ϕ in the latest QMC from the ϵ -expansion and conformal bootstrap, as shown in Table I.

Faced with these difficulties, here we work in a different direction. Instead of enlarging the linear region, we only simulate the linear region—the momentum space near the Dirac points—with the EMUS-QMC method [28,32,33]. The EMUS scheme is different from the usual fermion determi-

nant QMC, in that, instead of simulating the lattice model with a homogeneous $L \times L$ grid in real (and momentum) space, it focuses on small patches of BZ that are important in the IR limit and ignore the momenta elsewhere. In this Letter, we choose the patches to be two squares with side lengths $\frac{1}{6}$ of the full BZ centered at the Dirac points, where the dispersion deviates from the linear dispersion to within 5%. By simulating only $(L_f + 1)^2$ fermion modes in each patch, one effectively simulates a full system with size $L = 6L_f$. We note a larger ratio is not favored as in that case the patch will contain the momenta substantially deviated from the linear region and then introduce UV defects, and at the same time, although one can choose a small ratio to make the effective system size even larger, one would need to pay the price that the inverse temperature β would need to be scaled with L to probe the quantum critical point and the computation complexity linearly scales with β . Overall, the ratio of $\frac{L_f}{L} = \frac{1}{6}$ is found to be ideal for our model in Eq. (1).

Although the hard cutoff in momentum space effectively renders the QMC to simulate a different model—whose dispersion near the Dirac points is the same as the original one—with different finite-temperature observables, such as the values of the order parameter, we find the CFT data (critical properties) of the EMUS simulation share the same IR structure with the original ones, as shown in this Letter and our previous examples [28,32,33]. Previous studies have demonstrated the validity of the EMUS-QMC method, where it was shown that the simulated models with both the usual DQMC and EMUS-QMC give rise to the same universal information including the critical exponents and scaling form of bosonic propagators of the antiferromagnetic Ising critical points coupled to the Fermi surface [28,33]. Moreover, the EMUS-QMC scheme has been shown to successfully access the quantum critical data beyond the critical exponents; one example is Ref. [33], where various non-Fermi-liquid properties such as the Fermi-surface topology and self-energies are obtained.

As shown in Figs. 1(c) and 1(d), the momentum modes included in the simulation belong to two small patches near the Dirac points, where the dispersion is almost linear. When updating the bosonic field directly in momentum space, one only needs to keep track of the momentum transfer within the same patch, making the coupling terms grouped and block diagonal, instead of global and all-to-all, which is the case if one performs a local update in real space [28,32,33].

We leave the detailed description of the EMUS-QMC to the Supplemental Material (SM) [40], but just to highlight that we can now simulate system sizes up to $36 \times 36 \times 2$, with less computation time and human time, compared with the $16 \times 16 \times 2$ in traditional method [26].

Results. We perform EMUS-QMC on Eq. (1) with patch sizes $L_f = 2, 4, 6$, which leads to an equivalent full system size $L = 12, 24, 36$, and the inverse temperature is set to be proportional to the system size $\beta = \frac{3}{4}L$. We compute the magnetic structure factor of the bosonic field $S(\mathbf{q}) = \frac{1}{L^2} \langle \phi_{\mathbf{q}} \phi_{-\mathbf{q}} \rangle = \frac{1}{L^2} \sum_{i,j} e^{-i\mathbf{q} \cdot (\mathbf{r}_i - \mathbf{r}_j)} \langle \phi_i \phi_j \rangle$, and use $S(\Gamma)$ (square of the order parameter) and the RG-invariant correlation ratio $R = 1 - \frac{S(\Gamma + \Delta\mathbf{q})}{S(\Gamma)}$ [42], where $\Delta\mathbf{q} = \frac{2\pi}{L}(0, 1)$ or $(1, 0)$, to extract the GNY critical exponents. Since we work directly in momentum space, the Fourier components $\phi_{\mathbf{q}}$ can be used in measurements on the fly.

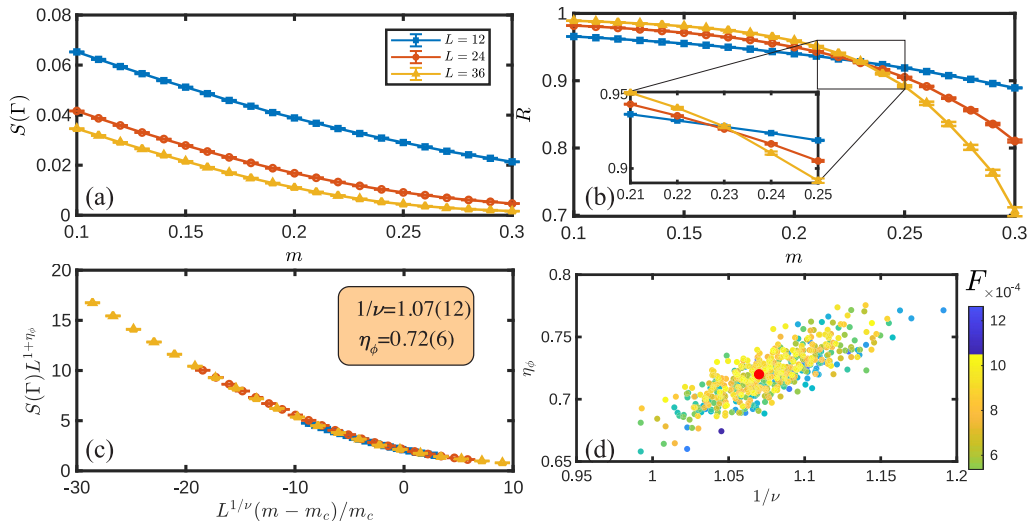


FIG. 2. $N = 8$ chiral Ising GNY CFT data. (a) The square of the bosonic order parameter $S(\Gamma)$, and (b) the correlation ratio R against the control parameter m for system sizes $L = 12, 24, 36$. (c) and (d) The data collapse of $S(\Gamma)$ vs m and the stochastic analysis of the error bound of $\{1/\nu, \eta_\phi\}$. Results yield $1/\nu = 1.07(12)$ and the bosonic anomalous dimension $\eta_\phi = 0.72(6)$. The color bar in (d) denotes the F ratio of deviation. The red dot is the set of exponents used in the collapse in (c).

One sees in Fig. 2(b) that the drift of crossing points of R is extremely small compare to that in Fig. 2 of Ref. [26]. This is a strong indication that our simulation has a smaller finite-size effect, as we attain larger effective system sizes. With the obtained $S(\Gamma)$ and R in Figs. 2(a) and 2(b), we further perform a stochastic data collapse in Figs. 2(c) and 2(d), to unbiasedly determine the optimized critical exponents $\{1/\nu, \eta_\phi\}$. The detailed description of such an analysis is given in SM [40], and here we outline the main procedure and results.

We sample the values of $\{1/\nu, \eta_\phi\}$ from the 2D parameter space in Fig. 2(d). Whenever a set of critical exponents is proposed, we try to fit a single curve with rescaled data from all system sizes [as in Fig. 2(c)], compute the ratio of deviation F to determine the goodness of fit, and vary the exponents until F attains its minimum. This whole process is repeated 1000 times with random noise added to $S(\Gamma)$ within its error bar and with random initial guesses in the $\{1/\nu, \eta_\phi\}$ space, so as to estimate the error bound for the optimal exponents, which is shown in Fig. 2(d). The color of each dot indicates its magnitude of convergent F ratio, where those of the blue ones are lower, and fit better. In this way, exponents $1/\nu = 1.07(12)$ and $\eta_\phi = 0.72(6)$ are obtained. The red dot indicates the exponents are generated from the original data of $S(\Gamma)$ without noise, which collapses well as shown in Fig. 2(c).

To obtain the fermion anomalous dimension η_ψ , we monitor the imaginary time Green's function by utilizing the Lorentz symmetry at the GNY-Ising CFT. Figure 3 shows the imaginary time decay of the fermionic and bosonic Green's function at the critical point m_c , where $G_f(\tau) = \frac{1}{L^2} \sum_{\mathbf{k}} \langle \psi_{\mathbf{k}}(\tau) \psi_{\mathbf{k}}^\dagger(0) \rangle$, and $G_b(\tau) = \frac{1}{L^2} \sum_{\mathbf{q}} \langle \phi_{\mathbf{q}}(\tau) \phi_{-\mathbf{q}}(0) \rangle$, respectively. Both panels are in log-log scale, and the dotted straight lines indicate the power-law decay of both correlation functions. From Fig. 3(a), we can extract the anomalous dimension of the fermion $\eta_\psi = 0.04(2)$, by the relation $G_f(\tau) \propto 1/\tau^{2+\eta_\psi}$, while in Fig. 3(b), a straight line of $G_b(\tau) \propto 1/\tau^{1.72}$ is drawn, using the $\eta_\phi = 0.72$ just obtained.

One can see both straight lines match well with the data as the system size L increases, which reflects the robustness of η_ψ and η_ϕ .

Discussion. Table I summarizes our results and the previous ones from QMC, ϵ expansion, and conformal bootstrap. One sees a textbook level consistency of the $\{1/\nu, \eta_\phi, \eta_\psi\}$ for the $N = 8$ chiral Ising GNY with the conformal bootstrap [9] and ϵ expansion [24] is finally achieved. We note that the present EMUS-QMC simulation actually consumes much less computation resources compared with our previous one [26], and it can be readily extended to other chiral GNY islands with different numbers of fermion flavors and symmetries of the bosonic field, by simply changing the power in the fermion determinant and the form of the boson energy difference [40].

The EMUS-QMC can also be used to investigate other GNY transitions from DSM to plaquette valence bond solids [43–47], SU(2) QSH [48–50], nematic order [13], intervalley

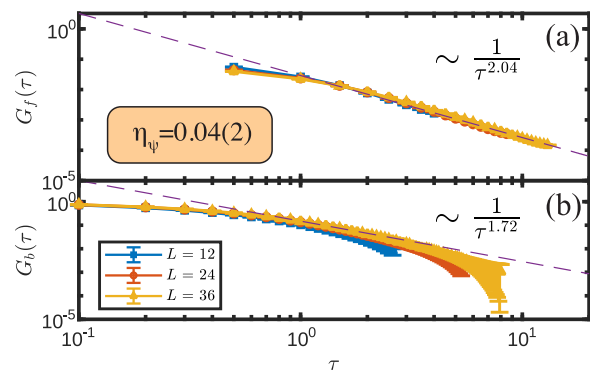


FIG. 3. Fermion and boson Green's functions at the chiral GNY CFT. We fit the imaginary time decays of (a) fermionic and (b) bosonic Green's functions, to extract the anomalous dimension $\eta_\psi = 0.04(2)$ and verify the consistency of $\eta_\phi = 0.72$ obtained from Fig. 2.

coherent and valley polarized orders [51–55], as well as superconductivity [56,57] in graphene and twisted bilayer graphene and kagome metal systems. It could also be applied to the investigations of the symmetric mass generation transitions in which the Dirac cones are gapped out without spontaneous symmetry breaking [58–62]. We foresee EMUS will soon explore the exciting islands in the vast ocean of CFTs and the broad continent of realistic 2D quantum materials.

Acknowledgments. We thank Junchen Rong and Ning Su for inspiring discussions on the GNY transition from a conformal bootstrap perspective, Michael Scherer for the enlightening education on the GNY transition from perturbative RG aspects, and Gaopei Pan and Weilun Jiang for useful technical suggestions on EMUS-QMC implementation. T.-T.W. and Z.Y.M. acknowledge support from the Research Grants Council (RGC) of Hong Kong Special Administra-

tive Region (SAR) of China (Projects No. 17301420, No. 17301721, No. AoE/P-701/20, No. 17309822, and No. HKU C7037-22G), the ANR/RGC Joint Research Scheme sponsored by the RGC of Hong Kong SAR of China and French National Research Agency (Project No. A_HKU703/22), the HKU Seed Funding for Strategic Interdisciplinary Research “Many-body paradigm in quantum moire material research”, and the Seed Funding “Quantum-Inspired explainable-AI” at the HKU-TCL Joint Research Centre for Artificial Intelligence. The authors acknowledge the HPC2021 system under the Information Technology Services and the Blackbody HPC system at the Department of Physics, University of Hong Kong for providing HPC resources. We also thank the Oasis High-performance computing under OneAsia Network for their technical support and generous allocation of CPU time.

-
- [1] D. F. Litim and D. Zappalà, Ising exponents from the functional renormalization group, *Phys. Rev. D* **83**, 085009 (2011).
- [2] M. V. Kompaniets and E. Panzer, Minimally subtracted six-loop renormalization of $O(n)$ -symmetric ϕ^4 theory and critical exponents, *Phys. Rev. D* **96**, 036016 (2017).
- [3] S. El-Showk, M. F. Paulos, D. Poland, S. Rychkov, D. Simmons-Duffin, and A. Vichi, Solving the 3D Ising model with the conformal bootstrap, *Phys. Rev. D* **86**, 025022 (2012).
- [4] F. Kos, D. Poland, D. Simmons-Duffin, and A. Vichi, Precision islands in the Ising and $O(N)$ models, *J. High Energy Phys.* **08** (2016) 036.
- [5] S. M. Chester, W. Landry, J. Liu, D. Poland, D. Simmons-Duffin, N. Su, and A. Vichi, Carving out OPE space and precise $O(2)$ model critical exponents, *J. High Energy Phys.* **06** (2020) 142.
- [6] S. M. Chester, W. Landry, J. Liu, D. Poland, D. Simmons-Duffin, N. Su, and A. Vichi, Bootstrapping Heisenberg magnets and their cubic instability, *Phys. Rev. D* **104**, 105013 (2021).
- [7] M. Hasenbusch, Finite size scaling study of lattice models in the three-dimensional Ising universality class, *Phys. Rev. B* **82**, 174433 (2010).
- [8] J. Gracey, Three-loop calculations in the $O(N)$ Gross-Neveu model, *Nucl. Phys. B* **341**, 403 (1990).
- [9] R. S. Erramilli, L. V. Iliesiu, P. Kravchuk, A. Liu, D. Poland, and D. Simmons-Duffin, The Gross-Neveu-Yukawa archipelago, *J. High Energy Phys.* **02** (2023) 036.
- [10] J. A. Gracey, T. Luthe, and Y. Schröder, Four loop renormalization of the Gross-Neveu model, *Phys. Rev. D* **94**, 125028 (2016).
- [11] N. Zerf, L. N. Mihaila, P. Marquard, I. F. Herbut, and M. M. Scherer, Four-loop critical exponents for the Gross-Neveu-Yukawa models, *Phys. Rev. D* **96**, 096010 (2017).
- [12] M. Vojta, Y. Zhang, and S. Sachdev, Quantum Phase Transitions in d -Wave Superconductors, *Phys. Rev. Lett.* **85**, 4940 (2000).
- [13] J. Schwab, L. Janssen, K. Sun, Z. Y. Meng, I. F. Herbut, M. Vojta, and F. F. Assaad, Nematic Quantum Criticality in Dirac Systems, *Phys. Rev. Lett.* **128**, 157203 (2022).
- [14] A. K. Geim and K. S. Novoselov, The rise of graphene, *Nat. Mater.* **6**, 183 (2007).
- [15] I. F. Herbut, Interactions and Phase Transitions on Graphene’s Honeycomb Lattice, *Phys. Rev. Lett.* **97**, 146401 (2006).
- [16] I. F. Herbut, V. Juričić, and B. Roy, Theory of interacting electrons on the honeycomb lattice, *Phys. Rev. B* **79**, 085116 (2009).
- [17] I. F. Herbut, V. Juričić, and O. Vafek, Relativistic Mott criticality in graphene, *Phys. Rev. B* **80**, 075432 (2009).
- [18] Y. Cao, V. Fatemi, S. Fang, K. Watanabe, T. Taniguchi, E. Kaxiras, and P. Jarillo-Herrero, Unconventional superconductivity in magic-angle graphene superlattices, *Nature (London)* **556**, 43 (2018).
- [19] Y. Cao, V. Fatemi, A. Demir, S. Fang, S. L. Tomarken, J. Y. Luo, J. D. Sanchez-Yamagishi, K. Watanabe, T. Taniguchi, E. Kaxiras *et al.*, Correlated insulator behaviour at half-filling in magic-angle graphene superlattices, *Nature (London)* **556**, 80 (2018).
- [20] D. M. Kennes, M. Claassen, L. Xian, A. Georges, A. J. Millis, J. Hone, C. R. Dean, D. N. Basov, A. N. Pasupathy, and A. Rubio, Moiré heterostructures as a condensed-matter quantum simulator, *Nat. Phys.* **17**, 155 (2021).
- [21] E. Y. Andrei, D. K. Efetov, P. Jarillo-Herrero, A. H. MacDonald, K. F. Mak, T. Senthil, E. Tutuc, A. Yazdani, and A. F. Young, The marvels of moiré materials, *Nat. Rev. Mater.* **6**, 201 (2021).
- [22] J.-X. Yin, B. Lian, and M. Z. Hasan, Topological kagome magnets and superconductors, *Nature (London)* **612**, 647 (2022).
- [23] M. Kang, L. Ye, S. Fang, J.-S. You, A. Levitan, M. Han, J. I. Facio, C. Jozwiak, A. Bostwick, E. Rotenberg, M. K. Chan, R. D. McDonald, D. Graf, K. Kaznatcheev, E. Vescovo, D. C. Bell, E. Kaxiras, J. van den Brink, M. Richter, M. Prasad Ghimire *et al.*, Dirac fermions and flat bands in the ideal kagome metal FeSn, *Nat. Mater.* **19**, 163 (2020).
- [24] B. Ihrig, L. N. Mihaila, and M. M. Scherer, Critical behavior of Dirac fermions from perturbative renormalization, *Phys. Rev. B* **98**, 125109 (2018).
- [25] L. Iliesiu, F. Kos, D. Poland, S. S. Pufu, and D. Simmons-Duffin, Bootstrapping 3D fermions with global symmetries, *J. High Energy Phys.* **01** (2018) 036.
- [26] Y. Liu, W. Wang, K. Sun, and Z. Y. Meng, Designer Monte Carlo simulation for the Gross-Neveu-Yukawa transition, *Phys. Rev. B* **101**, 064308 (2020).
- [27] S. Chandrasekharan and A. Li, Quantum critical behavior in three dimensional lattice Gross-Neveu models, *Phys. Rev. D* **88**, 021701(R) (2013).

- [28] Z. H. Liu, X. Y. Xu, Y. Qi, K. Sun, and Z. Y. Meng, Elective-momentum ultrasize quantum Monte Carlo method, *Phys. Rev. B* **99**, 085114 (2019).
- [29] Y.-Y. He, X. Y. Xu, K. Sun, F. F. Assaad, Z. Y. Meng, and Z.-Y. Lu, Dynamical generation of topological masses in Dirac fermions, *Phys. Rev. B* **97**, 081110(R) (2018).
- [30] S. M. Tabatabaei, A.-R. Negari, J. Maciejko, and A. Vaezi, Chiral Ising Gross-Neveu Criticality of a Single Dirac Cone: A Quantum Monte Carlo Study, *Phys. Rev. Lett.* **128**, 225701 (2022).
- [31] C. Bonati, A. Franchi, A. Pelissetto, and E. Vicari, Chiral critical behavior of 3D lattice fermionic models with quartic interactions, *Phys. Rev. D* **107**, 034507 (2023).
- [32] X. Y. Xu, Z. H. Liu, G. Pan, Y. Qi, K. Sun, and Z. Y. Meng, Revealing fermionic quantum criticality from new Monte Carlo techniques, *J. Phys.: Condens. Matter* **31**, 463001 (2019).
- [33] Z. H. Liu, G. Pan, X. Y. Xu, K. Sun, and Z. Y. Meng, Itinerant quantum critical point with fermion pockets and hotspots, *Proc. Natl. Acad. Sci. USA* **116**, 16760 (2019).
- [34] T. C. Lang and A. M. Läuchli, Quantum Monte Carlo Simulation of the Chiral Heisenberg Gross-Neveu-Yukawa Phase Transition with a Single Dirac Cone, *Phys. Rev. Lett.* **123**, 137602 (2019).
- [35] H. Nielsen and M. Ninomiya, Absence of neutrinos on a lattice: (I). Proof by homotopy theory, *Nucl. Phys. B* **185**, 20 (1981).
- [36] H. Nielsen and M. Ninomiya, Absence of neutrinos on a lattice: (II). Intuitive topological proof, *Nucl. Phys. B* **193**, 173 (1981).
- [37] J. A. Koziol, A. Langheld, S. C. Kapfer, and K. P. Schmidt, Quantum-critical properties of the long-range transverse-field Ising model from quantum Monte Carlo simulations, *Phys. Rev. B* **103**, 245135 (2021).
- [38] Y. Da Liao, X. Y. Xu, Z. Y. Meng, and Y. Qi, Caution on Gross-Neveu criticality with a single Dirac cone: Violation of locality and its consequence of unexpected finite-temperature transition, [arXiv:2210.04272](https://arxiv.org/abs/2210.04272).
- [39] Z. Wang, F. Assaad, and M. Ulybyshev, Validity of SLAC fermions for the $(1+1)$ -dimensional helical Luttinger liquid, *Phys. Rev. B* **108**, 045105 (2023).
- [40] See Supplemental Material at <http://link.aps.org/supplemental/10.1103/PhysRevB.108.L121112> for a detailed discussion on the concept and implementation of the elective-momentum ultrasize (EMUS)-QMC method, and details on how to perform the stochastic data collapse to unbiasedly extract the critical exponents, which includes Ref. [41].
- [41] L. Wang, K. S. D. Beach, and A. W. Sandvik, High-precision finite-size scaling analysis of the quantum-critical point of $S=12$ Heisenberg antiferromagnetic bilayers, *Phys. Rev. B* **73**, 014431 (2006).
- [42] S. Pujari, T. C. Lang, G. Murthy, and R. K. Kaul, Interaction-Induced Dirac Fermions from Quadratic Band Touching in Bilayer Graphene, *Phys. Rev. Lett.* **117**, 086404 (2016).
- [43] T. Sato, M. Hohenadler, and F. F. Assaad, Dirac Fermions with Competing Orders: Non-Landau Transition with Emergent Symmetry, *Phys. Rev. Lett.* **119**, 197203 (2017).
- [44] Y. Ouyang and X. Y. Xu, Projection of infinite- U Hubbard model and algebraic sign structure, *Phys. Rev. B* **104**, L241104 (2021).
- [45] Y. D. Liao, X. Y. Xu, Z. Y. Meng, and Y. Qi, Dirac fermions with plaquette interactions. I. SU(2) phase diagram with Gross-Neveu and deconfined quantum criticalities, *Phys. Rev. B* **106**, 075111 (2022).
- [46] Y. D. Liao, X. Y. Xu, Z. Y. Meng, and Y. Qi, Dirac fermions with plaquette interactions. II. SU(4) phase diagram with Gross-Neveu criticality and quantum spin liquid, *Phys. Rev. B* **106**, 115149 (2022).
- [47] Y. D. Liao, X. Y. Xu, Z. Y. Meng, and Y. Qi, Dirac fermions with plaquette interactions. III. SU(N) phase diagram with Gross-Neveu criticality and first-order phase transition, *Phys. Rev. B* **106**, 155159 (2022).
- [48] Y. Liu, Z. Wang, T. Sato, M. Hohenadler, C. Wang, W. Guo, and F. F. Assaad, Superconductivity from the condensation of topological defects in a quantum spin-Hall insulator, *Nat. Commun.* **10**, 2658 (2019).
- [49] Z. Wang, Y. Liu, T. Sato, M. Hohenadler, C. Wang, W. Guo, and F. F. Assaad, Doping-Induced Quantum Spin Hall Insulator to Superconductor Transition, *Phys. Rev. Lett.* **126**, 205701 (2021).
- [50] Z. H. Liu, W. Jiang, B.-B. Chen, J. Rong, M. Cheng, K. Sun, Z. Y. Meng, and F. F. Assaad, Fermion Disorder Operator at Gross-Neveu and Deconfined Quantum Criticalities, *Phys. Rev. Lett.* **130**, 266501 (2023).
- [51] Y. Da Liao, Z. Y. Meng, and X. Y. Xu, Valence Bond Orders at Charge Neutrality in a Possible Two-Orbital Extended Hubbard Model for Twisted Bilayer Graphene, *Phys. Rev. Lett.* **123**, 157601 (2019).
- [52] Y. D. Liao, J. Kang, C. N. Breið, X. Y. Xu, H.-Q. Wu, B. M. Andersen, R. M. Fernandes, and Z. Y. Meng, Correlation-Induced Insulating Topological Phases at Charge Neutrality in Twisted Bilayer Graphene, *Phys. Rev. X* **11**, 011014 (2021).
- [53] Y.-D. Liao, X.-Y. Xu, Z.-Y. Meng, and J. Kang, Correlated insulating phases in the twisted bilayer graphene, *Chin. Phys. B* **30**, 017305 (2021).
- [54] G. Pan, X. Zhang, H. Li, K. Sun, and Z. Y. Meng, Dynamical properties of collective excitations in twisted bilayer graphene, *Phys. Rev. B* **105**, L121110 (2022).
- [55] G. Pan, W. Jiang, and Z. Y. Meng, A sport and a pastime: Model design and computation in quantum many-body systems, *Chin. Phys. B* **31**, 127101 (2022).
- [56] X. Y. Xu and T. Grover, Competing Nodal d -Wave Superconductivity and Antiferromagnetism, *Phys. Rev. Lett.* **126**, 217002 (2021).
- [57] X. Zhang, K. Sun, H. Li, G. Pan, and Z. Y. Meng, Superconductivity and bosonic fluid emerging from moiré flat bands, *Phys. Rev. B* **106**, 184517 (2022).
- [58] K. Slagle, Y.-Z. You, and C. Xu, Exotic quantum phase transitions of strongly interacting topological insulators, *Phys. Rev. B* **91**, 115121 (2015).
- [59] V. Ayyar and S. Chandrasekharan, Massive fermions without fermion bilinear condensates, *Phys. Rev. D* **91**, 065035 (2015).
- [60] S. Catterall, Fermion mass without symmetry breaking, *J. High Energy Phys.* **01** (2016) 121.
- [61] Y.-Y. He, H.-Q. Wu, Y.-Z. You, C. Xu, Z. Y. Meng, and Z.-Y. Lu, Quantum critical point of Dirac fermion mass generation without spontaneous symmetry breaking, *Phys. Rev. B* **94**, 241111(R) (2016).
- [62] Z. H. Liu, Y. Da Liao, G. Pan, W. Jiang, C.-M. Jian, Y.-Z. You, F. F. Assaad, Z. Y. Meng, and C. Xu, Disorder operator and Rényi entanglement entropy of symmetric mass generation, [arXiv:2308.07380](https://arxiv.org/abs/2308.07380).